

# Energy redistribution between layers in multi-layered target heated by x-ray pulse

N A Inogamov<sup>1,2</sup>, V A Khokhlov<sup>1</sup>, V V Zhakhovsky<sup>2</sup> and Yu V Petrov<sup>1</sup>

<sup>1</sup> Landau Institute for Theoretical Physics of the Russian Academy of Sciences, Akademika Semenova 1a, Chernogolovka, Moscow Region 142432, Russia

<sup>2</sup> Dukhov Research Institute of Automatics (VNIIA), Sushchevskaya 22, Moscow 127055, Russia

E-mail: [nailinogamov@gmail.com](mailto:nailinogamov@gmail.com)

**Abstract.** Multi-layered systems with alternated layers of different materials (laminates) with thickness of the order of tens nanometers are widely used in modern technologies, e.g., as x-ray mirrors. It is important to study effect of the x-ray free electron lasers on such targets. High-energy photons penetrate deeply into material with an attenuation depth much larger than the thickness of a single layer of a laminate. Modern hard x-rays lasers may be focused to tiny focal spots in the direction approaching diffraction limit: record today is  $\approx 50$  nm;  $\sim 1$   $\mu$ m diameters are now rather easily achieved. These lasers may be used for machining of laminates. We show that thermal evolution of illuminated laminates depends on not only photon absorption in the individual materials, but also on fast redistribution of absorbed energy within a nonequilibrium stage connected with electron-ion relaxation (two-temperature stage) between hot electrons heated by absorption and much colder ions. Because of the high heat conductivity of metal layers, especially at the two-temperature stage, energy redistribution must be considered with taking into account the energy transfer from electrons to ions with different electron-ion coupling parameters  $\alpha$  for different metals. Thus, a higher energy can be localized in a material with higher  $\alpha$  rather than in a material with higher photon absorption coefficient.

## 1. Introduction

The layered structures are used in different applications, in particular as the x-ray mirrors for extreme ultraviolet and soft x-rays. Their wavelengths are from few to tens nanometers. These mirrors are layered systems with thickness of a layer of the order of the wavelength of radiation that should be reflected. Damage or lithographic processing of the layered mirrors by a pulse of hard x-rays is considered in this paper.

We study action of very short pulse with duration  $\sim 10$  fs produced at XFELs (x-ray free electron lasers) such as RIKEN SACLA [1] or DESY [2]. In the case of an ultrashort pulse the two-temperature (2T) stage becomes important; there is large temperature difference between electrons and ions at this stage. There is significant redistribution of absorbed energy between layers of two different metals at the 2T stage.

At the 2T stage the high metallic thermal conductivity  $\kappa$  becomes even more high [3–6]; for gold  $\kappa_{2T}$  may achieve values of few  $10^3$   $\text{WK}^{-1}\text{m}^{-1}$  [4] while  $\kappa_{1T} \approx 300$   $\text{WK}^{-1}\text{m}^{-1}$  for solid Au. Thermal diffusivity  $\chi$  is from a few times to order of magnitude times *larger* than its one-temperature (1T) value  $\chi_{1T}$  equal  $\chi_{1T} \approx 1$   $\text{cm}^2/\text{s}$  for typical metals. Therefore, thermal



**Figure 1.** Structure of our 5-layered target deposited onto thick silicon substrate.

energy is quickly transported outside from a hot layer with high absorption coefficient (= shorter attenuation depth). The hot layers at the end of the 10 fs absorption stage are the gold layers in figure 1. Gold has more electrons per atom and deeper electron shells than Cr therefore Au better absorbs hard photons.

High values of  $\kappa_{2T}$  and  $\chi_{2T}$  are responsible for supersonic propagation of an electron thermal wave during a time interval approximately corresponding to the 2T stage [3,7,8]; see also figure 1 in [9] where (i) the short stage of supersonic propagation of heat, (ii) its transfer to subsonic regime, and (iii) irradiation of acoustic wave at the transonic transition between supersonic and subsonic expansion of heat are emphasized. Thus the compression wave starts not from a vacuum boundary but from the rather deep penetrated edge of the thermal wave.

The situation is similar to the early mainly radiative expansion of light ball caused by atomic explosion; shock only later separates and overruns the hot ball. In both cases the leading position of supersonic thermal wave (photonic or electronic) is caused by high velocities of the heat carriers (photons-speed of light or electrons-Fermi velocity) moving much faster than ions. In this regime Knudsen number  $Kn \ll 1$  is small (collisional case), thus this is diffusive propagation and truly thermal wave (not a ballistic expansion of hot photons or electrons when  $Kn \sim 1$  before the first collisions).

Electron thermal energy transported from Au layers into surrounding Cr layers in figure 1 is mostly transferred to ionic subsystem of the metal with higher electron-ion coupling parameter  $\alpha$ ; this is Cr. Thus conduction and coupling strongly redistribute absorbed energy between the Au and Cr layers. The effect of preferable heating of ions in a contacting metal with higher value of coupling parameter  $\alpha$  was studied in paper [10]. The case of two layers one of Au and other of Cu has been analyzed [10]. There was an Au layer 30 nm thick deposited onto bulk Cu. Light comes to vacuum boundary of Au. Optical radiation is absorbed in a skin-layer of gold. The skin is thinner than thickness of Au film. Thus almost all laser energy is initially deposited into electron subsystem of Au. But high conduction in gold and fast electron-ion coupling in Cu lead to melting beginning in Cu, not in the heated Au, although melting temperature of Cu is slightly higher: 20 K difference, i.e. 1357 versus 1337 K.

Hard x-ray is weakly reflected from substance, with exception of grazing incidence. Astrophysics telescopes mounted on satellites (for example XMM-Newton, Spektr-RG) are based on low-angle reflection. Refractive index of gold is very close to unit:  $N = n + ik = (1 - \delta) + ik$ ,  $\delta = 5.15 \times 10^{-5}$ ,  $k = 5.67 \times 10^{-6}$  (Henke tables), at photon energy 7.71 keV. Therefore the reflection coefficient from a bulk target of gold is negligible for normal incidence:

$$R = \frac{(n-1)^2 + k^2}{(n+1)^2 + k^2} = \frac{1}{4}(\delta^2 + k^2) \approx \frac{1}{4}\delta^2 = 6.7 \times 10^{-10}.$$

The reflection coefficient increases on many orders with the help of multi-layered systems, also called as laminates. Laminate with layer thickness  $a$  of the order of wavelength  $\lambda_{\text{ref}}$ , which is required to reflect, works like a 1D photon crystal. Let A and B a pair of materials in neighbor layers. Reflection coefficients  $R$  for both A and B are very small and they are smooth functions of wavelengths beyond the top energies of electron shells. Contrary, the resonances appear in photon crystal, and a band structure on the length  $\lambda$  appears with them. The structure consists of permitted bands and band-gaps. By adjusting the thickness  $a$  corresponding to the particular refraction indices  $N_A$ ,  $N_B$ , one can achieve the situation when the wavelength  $\lambda_{\text{ref}}$  falls into a band gap.

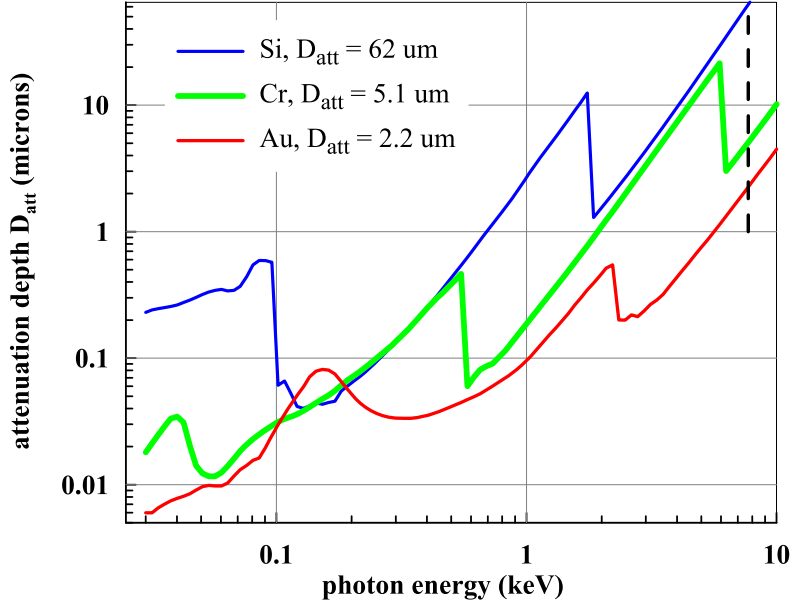


**Figure 2.** Spectrum of absorptance (Henke tables) [11]. The values of  $D_{\text{att}}(E)$  for the energy  $E = 7.71$  keV (this energy is marked by the vertical dashed line) are shown. Three curves relate to three substances used in figure 1, see the legend in the upper left corner of the picture.

Then the wave with  $\lambda_{\text{refl}}$  cannot penetrate into the multi-layered system. Its reflection coefficient  $R(\lambda_{\text{refl}})$  becomes of the order of 1:  $R(\lambda_{\text{refl}}) \leq 1$ , i.e. it exceeds  $R_A, R_B$  for reflection from the bulk targets of substance A or B.

The layered x-ray mirrors with thickness of  $a \sim 10$  nm are intended for soft x-ray with photon energy of tens hundreds eV. The reflection coefficient from the bulk gold target is  $R = 0.004$  (0.4%),  $\delta = 0.1$ ,  $k = 0.06$  (Henke tables) for the wavelength of 13.9 nm with photon energy of about 90 eV. The disadvantage of multi-layered mirror is in a specific  $\lambda_{\text{refl}}$  for which it was designed. For other wavelengths this mirror is not applicable.

Light with wavelength 13.5 nm from tin plasma is used for high spatial density EUV lithography production of the most advanced integrated circuits [12, 13]. The focusing system of lithographic machines consists of several mirrors. The problem of damage of multi-layered mirrors by a hard irradiation arises. As was said above, there are possibilities to thermo-mechanically treat these mirrors by hard x-ray lasers.

In our work the effect of hard x-ray with photon energy  $\sim 10$  keV on a multi-layered system with thickness of layer  $a = 50$  nm is studied. Attenuation length  $D_{\text{att}}$  of such radiation is much longer than the layer thickness  $a$  ( $D_{\text{att}}$  is of the order of microns). But the absorption coefficients of the substances Au and Cr differ, figure 2. This is why the heating of electron subsystems by absorption of external irradiation differs too. And the heating pulse is ultrashort for free electron lasers such as SACLA (RIKEN x-ray Free Electron Laser ‘‘SACLA’’) [1] and DESY [2] having pulse duration  $\tau_L$  of few or few tens of fs (femtoseconds). In such conditions the redistribution of absorbed energy takes place between the layers. The redistribution proceeds after finishing of the heating laser pulse. In particular the hottest layer after 2T relaxation may have a lower coefficient of x-ray absorption.

Why is the 2T stage in a focus of our research? It is because the electron heat conductivity  $\kappa_{2T} \approx \kappa_{\text{rt}} T_e / T_i$  and temperature diffusivity  $\chi_e$  are higher within this stage where  $T_e \gg T_i$ . Here  $\kappa_{\text{rt}}$  is the electron heat conductivity at room temperature. The formula  $\kappa_{2T} \propto T_e / T_i$  is applicable if electron–electron collision frequency is lower than the electron–ion collision frequency [4, 6].

The value  $\chi_e|_{2T} = \kappa_{2T}/c_e$  is higher by 5–15 times than  $\kappa_{rt}/(c_i + c_e) \approx \kappa_{rt}/c_i \sim 1 \text{ cm}^2/\text{s}$ , where

$$c_i \approx 3k_B n, \quad c_e = (\pi^2/2)Z n k_B (k_B T_e/E_F)$$

are heat capacities of ions and electrons, respectively

$$c_e/c_i = (\pi^2/6)Z(k_B T_e/E_F).$$

Here  $n$  is ion concentration,  $Z$  is number of conduction electrons per atom,  $E_F$  is Fermi energy.

Heat propagates on distance  $\sqrt{\chi_e t_{\text{eq}}} \sim 140 \text{ nm}$  ( $\chi = 10 \text{ cm}^2/\text{s}$ ,  $t_{\text{eq}} \sim 2 \text{ ps}$ ) for a time of the order of duration of 2T stage. In simulations presented below we perform calculations of heat propagation on 2T and 1T stages until beginning of a stage of hydrodynamic decay and fragmentation of the multi-layered target.

## 2. Problem setup

Let's consider a five-layered system on a substrate from silicon. It consists of two layers of gold alternating with three layers of chrome. Wherein two of the three chrome layers are external to the five-layered coating of the substrate, and one chrome layer is in the middle plane of the structure, see figure 1. The boundary chrome layer at the interface with silicon significantly increases the adhesion of the structure to the substrate. This eliminates the delamination from the substrate structure in contrast to a structure where a gold film is on a substrate (then detachment from substrate is possible [14, 15]).

2T system of heat equations has the following form:

$$\rho \frac{\partial(E_e/\rho)}{\partial t} = \frac{\partial q}{\partial x} - \alpha(T_e - T_i) + P; \quad q = -\kappa \frac{\partial T_e}{\partial x}; \quad (1)$$

$$\rho \frac{\partial(E_i/\rho)}{\partial t} = \alpha(T_e - T_i). \quad (2)$$

The system of two separated energy balances for the electron (1) and the ion subsystems (2) is obtained by splitting of the one-temperature (1T) heat equation [16]; see also 2T hydrodynamics equations [17–20]. Here  $E_e$ ,  $E_i$  are internal energy of electrons and ions per unit volume, respectively,  $q$  is heat flux carried by electrons, the coefficient  $\alpha$  determines the rate of energy exchange between the electron and ion subsystems. Source term  $P$  associated with absorption of the x-ray pulse provides the heating power of electron subsystem per unit of volume. The function  $P(x, t)$  is homogeneous within the layers of one type in the calculations. It is given as a Gaussian function  $\propto \exp(-t^2/\tau_L^2)$  with a width  $\tau_L = 10 \text{ fs}$ ; this is e-folding time measured from the maximum, FWHM width is  $t_{\text{FWHM}} = 2\sqrt{\log 2} \tau_L$ . As we see the time origin is measured from the top point of the Gaussian.

## 3. Characteristics of materials

### 3.1. Absorption of hard radiation

Attenuation depth  $D_{\text{att}}(E)$  of the radiation intensity as functions of the photon energy  $E$  are shown in figure 2. The thermal calculations discussed below are based on assumption that the ratio of bulk density of absorbed power in gold, chromium and silicon correlates as 100 : 43 : 3.5 respectively, which is inversely proportional to the  $D_{\text{att}}$  taken from figure 2. Two variants are considered: one with a bulk power  $P = 1.37 \times 10^{24} \text{ W/m}^3$  of absorption in gold and the other with a bulk power  $P = 2.42 \times 10^{24} \text{ W/m}^3$ . Power  $P$  is included as a heat source in the equation (1). Bulk energy densities deposited in gold within 10 fs of x-ray action are 13.7 GPa and 24.2 GPa in these two cases.

The pulse duration of 10 fs is small compared to the time of electron–ion relaxation (of the order of picoseconds for chrome, for gold this time is longer) and time of heat transfer from layer to layer. Therefore, almost all absorbed energy is concentrated in the electron subsystems of

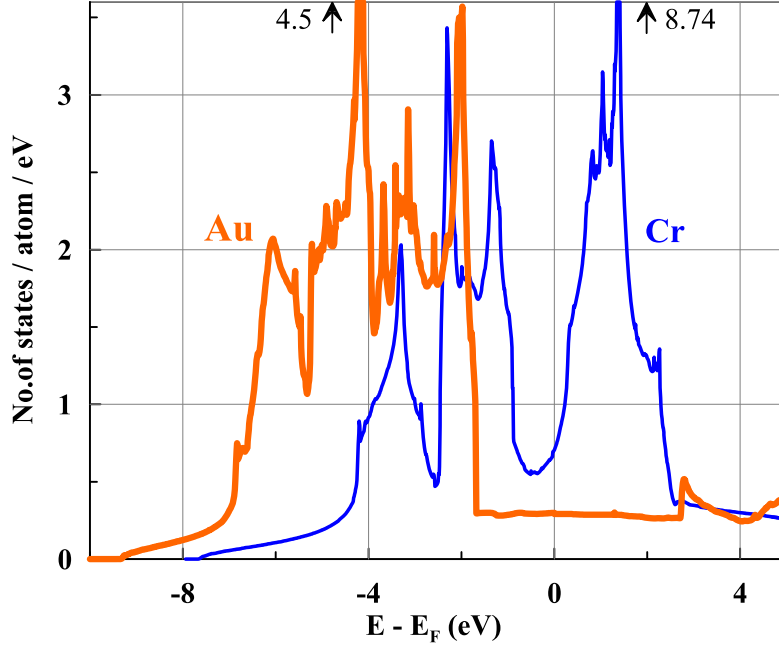


**Figure 3.** Band structure of gold  $4f^{14}5d^{10}6s^1$  and chrome  $3d^54s^1$  at their normal density of 19.3 and 7.19 g/cm<sup>3</sup>, respectively; 4f band of Au is not shown because it is located far away to the left side relative to the frame of energies shown here. Electron densities of states (DoS) as functions of the energy  $g(E)$  are shown;  $E_F = \mu(0)$  is the Fermi energy,  $\mu(T_e)$  is the chemical potential. Calculations of the DoS  $g(E; T_e, \rho)$  for the fcc and bcc Au and Cr crystal lattices are performed for a low electron temperature and the room temperature densities using the VASP package [4,5,21,22]. The arrows above mark the left and right edges of the d-band for Cr. They are below and above  $E_F$  for Cr.

gold, chromium and silicon by the end of the pulse. Then the heat transfer and e-i relaxation start.

Hard photon basically knocks out an electron from a deep shell, which is the nearest in energy to the the photon energy, see figure 2. Thus, most of the energy is in the form of potential energy of the deep holes, and less energy is converted into addition to kinetic energy of motion of electrons in a conduction band. This situation exists short time. Further, for tens of femtoseconds followed by Auger processes in which the potential energy of a hole decreases—hole “rises up” on the energy axis—and new knocked-on fast electrons appear. Then a hole is closed—all the absorbed energy is transferred into kinetic energy of the conduction band electrons. For gold, this energy is about 1.4 eV/atom at the energy density of 13.7 GPa and 2.5 eV/atom at heating to 24.2 GPa.

Electron energies came out rather great, the temperature  $T_e$  is 10–20 kK after electron-electron relaxation. Under these conditions, the rate of electron-electron collisions is high, the time between collisions is of the order of a few femtoseconds. Hence, the thermalization of the electron subsystem in gold and chrome finishes long before the end of the e-i relaxation. This justifies the use of 2T model (1), (2) from the very beginning.

Electron-hole pairs still can remain in silicon. But the influence of the silicon substrate on the overall energy balance is insignificant because of the small energy absorbed there and the relatively small (compared to the  $\kappa_{2T}$  in metals) thermal conductivity.

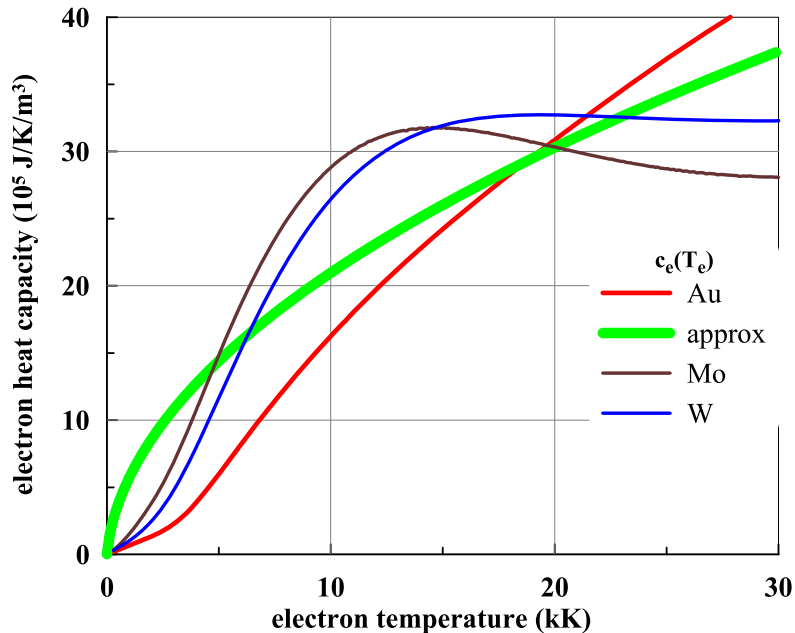


**Figure 4.** Electron heat capacities as functions  $T_e$  for gold, molybdenum and tungsten according to [21, 24]. DoS  $g(E, T_e = 0, \rho_{rt})$  are used for calculations, displacement of bands at variation of  $T_e$  is neglected. Approximating formula is given in the text. The value of  $25 \times 10^5$  J/K/m<sup>3</sup> corresponds to the Dulong–Petit law  $3k_B$  at Pippard concentration  $n = 6 \times 10^{22}$  cm<sup>3</sup>. In the range 10–20 kK of  $T_e$  the heat capacity  $c_e$  becomes an order of an ion heat capacity.

### 3.2. Electron Spectra and Thermodynamics

Bands of conductivity in gold and chrome are presented in figure 3. Their Fermi energies counted from a bottom of s-band, are equal 9.2 eV and 7.6 eV, respectively. The upper edge of the d-band is located below the Fermi surface in gold. Density functional theory calculation (DFT) using the VASP package [4, 5, 21, 22] underestimates the distance  $E_2$  to the top of the d-band: the package gives 1.7 eV instead of experimentally established values of 2.3–2.5 eV [23]. The chrome d-band is complex. It is split into parts above and below the Fermi energy  $E_F$ , see figure 3, thus forming the pseudo-gap (the well in DoS) around Fermi level.

The simplest method is an approximate calculation of the electron energy from the one-particle formula

$$\varepsilon(T_e, \rho) = \int_{-\infty}^{\infty} g(\varepsilon) f(\varepsilon, T_e, \mu(T_e)) \varepsilon d\varepsilon,$$

here  $g$ ,  $f$ ,  $\mu$  are density of states, the Fermi distribution, and the chemical potential, respectively [4, 5, 21, 22]. The chemical potential is determined from the normalization condition on the number of electrons in the conduction band.

Double counting of the Coulomb energy of the electron-electron interaction is neglected in such calculation [28]. Differentiation of energy gives the heat capacity  $c_e$ . Electron heat capacity as functions of temperature at the fixed normal density are shown in figure 4. Data are taken from a site [21, 24]. Molybdenum and tungsten have a complicated d-band, similar to the spectrum of chrome. We believe that the specific heat of chrome approximately corresponds to ones in Mo and W. We can see that the heat capacity of the three metals in figure 4 is not much

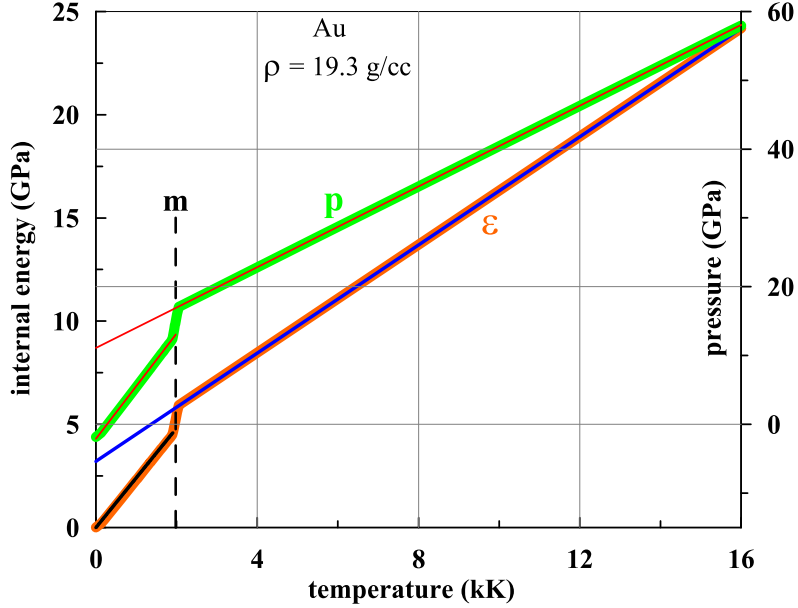


**Figure 5.** Energy  $\varepsilon$  (the left axis) and pressure  $p$  (the right axis) in gold as functions of the temperature  $T$  according to [25–27] and the corresponding linear approximations of those functions, see discussion in the text.

different. On this basis, we build the general approximating curve  $c_e(T_e)$ :

$$c_e(T_{\text{ekK}}) = C \left( \frac{T_1}{T_{\text{ekK}}} + \frac{T_2}{\sqrt{T_{\text{ekK}}}} \right)^{-1}, \quad (3)$$

where  $C = 10^5 \text{ J}/(\text{K m}^3)$ ,  $T_1 = 0.034 \text{ kK}$ ,  $T_2 = 0.14 \text{ kK}^{0.5}$ . Electron temperature  $T_e$  should be taken in kK units in the approximation (3), see the curve *approx* in figure 4.

Let us integrate the approximating curve (3), shown in figure 4. As a result, we obtain the required energy dependence of electron energy on electron temperature  $\varepsilon_e(T_e)$ :

$$\varepsilon_e = A \left[ A_1 \sqrt{T_{\text{ekK}}} - A_2 T_{\text{ekK}} + A_3 T_{\text{ekK}}^{3/2} - B \ln(B_1 + \sqrt{T_{\text{ekK}}}) \right], \quad (4)$$

$T_{\text{ekK}}$  is  $T_e$  in kK units,  $A = 0.1 \text{ GPa}$ ,  $A_1 = 0.84$ ,  $A_2 = 1.73$ ,  $A_3 = 4.76$ ,  $B = 0.2$ ,  $B_1 = 0.24$ . As it is possible to check up, the logarithm in the formula (4) at our temperatures  $T_e$  is small. Therefore it is rejected thereafter.

Equating the expression (4) to energies 13.7 GPa and 24.2 GPa, transmitted to the electron subsystem by x-ray pulse in the first and second variants, we find the maximum electron temperature of 10 and 14.5 kK in gold in these cases. Taking into account that 43% of the energy gets chrome, see section 3.1, we define the maximum electron temperature in the chrome 6 and 8.4 kK in these cases.

### 3.3. One-temperature thermodynamics and the ion contribution

The total energy is a sum of the electron and ion energies  $\varepsilon = \varepsilon_e + \varepsilon_i$ , where  $\varepsilon_e$  is from equation (4). The ion energy of gold at isochore density in normal conditions  $\rho_{\text{rt}}$  is taken from a wide-range equation of state [25–27]. 1T functions of internal energy and pressure on this isochore are presented in figure 5. We see that out of a narrow melting region  $m$ , the above functions are well described by the linear functions:  $\varepsilon_{\text{sol}} = 2.41 T_{\text{kK}}$ ,  $\varepsilon_{\text{liq}} = 1.31 T_{\text{kK}} + 3.21$ ,  $p_{\text{sol}} = 7.65 T_{\text{kK}} - 2.1$ ,  $p_{\text{liq}} = 2.934 T_{\text{kK}} + 11.1$  all in GPa.

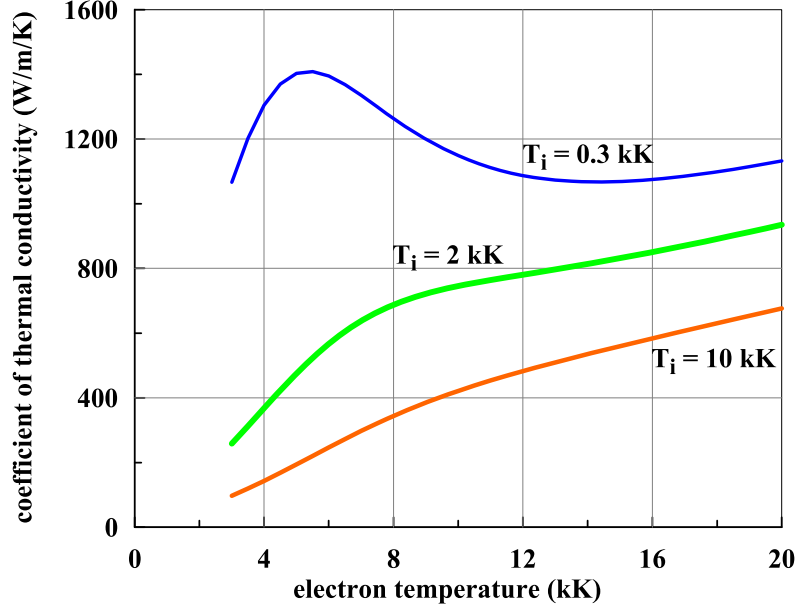


**Figure 6.** Thermal conductivity of gold in 2T conditions. Let us consider the function  $\kappa(T_e, T_i = 0.3 \text{ kK})$ . At a relatively small  $T_e$  this coefficient increases with  $T_e$  due to the partial removal of degeneracy and the growth of electron heat capacity (figure 4), since the frequency of s-i scattering does not change (temperature  $T_i$  is fixed), and the frequency of s-s and s-d scattering is small. With the growth of  $T_e$  frequencies  $\nu_{ss}, \nu_{sd}$  increase. The maximum of  $\kappa$  appears at the temperature  $T_e$ , on which the sum of  $\nu_{ss} + \nu_{sd}$  reaches  $\nu_{si}$ .

Melting on isochorus occurs under pressure, because the density is fixed. Temperature is higher than the  $T_m|_{p=0} = 1.337 \text{ kK}$  at the triple point while crossing the region between the solidus and liquidus. Isochore  $\rho_{rt} = 19.3 \text{ g/cm}^3$  enters the melting region at  $1.89 \text{ kK}$  and pressure  $p = 12.4 \text{ GPa}$  and leaves into a pure melt at  $T = 2.057 \text{ kK}$  and  $p = 9.16 \text{ GPa}$ . Width of intersection of the segment is  $164 \text{ K}$  on temperature and  $4.5 \text{ GPa}$  on pressure. The energy per unit volume is changed from  $4.489$  to  $5.927 \text{ GPa}$ , i.e. by  $1.44 \text{ GPa}$ . We assume that all of this energy is utilized in melting; i.e. the heating of solid-melt phase mixture is neglected. Then the heat of melting along isochors  $\rho_{rt}$  is  $1.44 \text{ GPa}$  or  $0.15 \text{ eV/atom}$  or  $14 \text{ kJ/mol}$  as shown in figure 5. The heat of melting for  $p = 0$  is  $12.6 \text{ kJ/mol}$  from the reference book. If we straighten dependence  $\varepsilon(T)$  in figure 5 in the melting region, the effective heat capacity per atom will be  $10.5k_B$ . Heat capacity increase is due to the heat of melting.

The heat capacities of the solid and liquid phases equal  $2.9k_B$  and  $1.6k_B$  respectively, in accordance with figure 5, and the Grüneisen parameters of these phases of gold are  $3.17$  and  $2.24$ . A dependence of  $\varepsilon(T)$  is necessary for thermal calculation with chrome. Both gold and chrome are melted at considered here values of absorbed energies. Therefore, the dependence  $\varepsilon_{\text{liq}}(T)$  is required for chrome. The concentration of atoms of chrome under normal conditions  $8.3 \times 10^{22} \text{ cm}^{-3}$  is significantly higher than  $5.9 \times 10^{22} \text{ cm}^{-3}$  in gold. Assume that heat capacity in the liquid chromium is approximately equal to  $1.6k_B$ . Then, up to a constant, we have  $\varepsilon_{\text{liq}}(T)|_{\text{Cr}} = 1.84T_{\text{kK}} + 3 \text{ GPa}$ . In the 2T thermal calculations we assume that the formulas given in this section describe ion contribution to the energy  $\varepsilon_i(T_i)$ , which depends on the ion temperature.

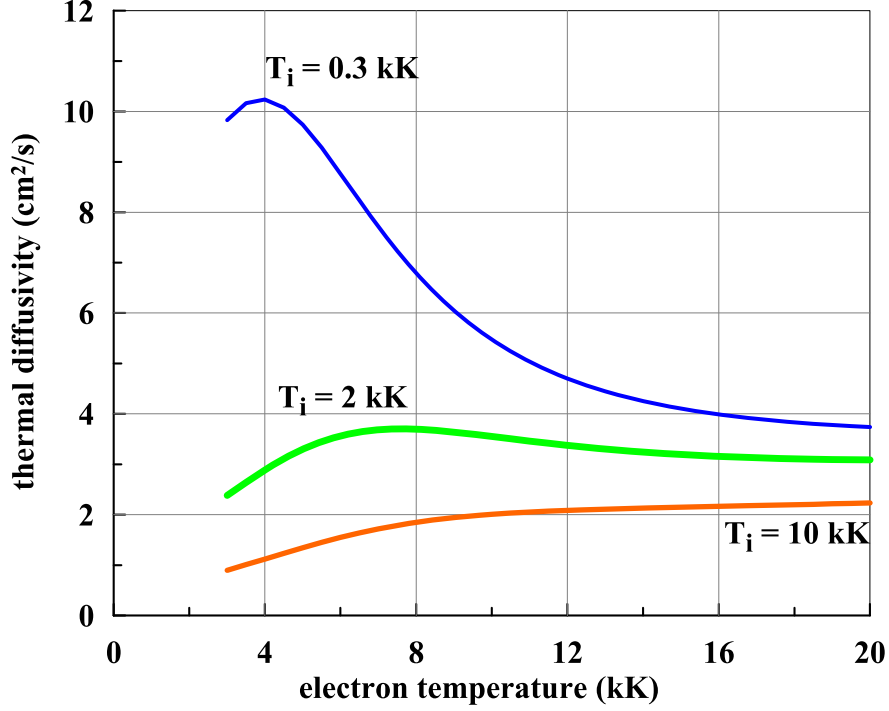


**Figure 7.** The thermal diffusivity  $\chi(T_e, T_i) = \kappa(T_e, T_i)/C_e(T_e)$ .

### 3.4. Heat conductivity

We will calculate the thermal conductivity of gold by the following formulas. The Fermi energy is  $E_{\text{FkK}} = 107$  in kK units (9.2 eV, see figure 3). Then we introduce the dimensionless electron temperature normalized to the Fermi energy:

$$t = \frac{6T_{\text{ekK}}}{E_{\text{FkK}}},$$

where  $T_{\text{ekK}}$ —electron temperature in kK. Approximation of the electron contribution to the thermal resistance has the form

$$S_{\text{se}} = \frac{S_0 t}{1 - S_q \sqrt{t} + S_1 t + S_2 t^2},$$

in units of [K m/W],  $S_0 = 3.8 \times 10^{-4}$ ,  $S_q = 2$ ,  $S_1 = 1.4$ ,  $S_2 = 0.04$ .

The thermal conductivity associated with the scattering of the s-electron on ions (i—ion, “s-i” or “si”), equal to

$$\kappa_{\text{si}}|_{\text{liq}} = 140 \frac{C(T_{\text{ekK}})}{C(T_{\text{mkK}})} \frac{w(T_{\text{mkK}})}{w(T_{\text{ikK}})}, \quad T_{\text{mkK}} = 1.337 \text{ kK}$$

in  $\text{WK}^{-1} \text{m}^{-1}$ .

There auxiliary functions are equal

$$C(T_{\text{ekK}}) = t \frac{1 + C_1 t^2}{1 + C_2 t^{2.05}}, \quad C_1 = 11.2, \quad C_2 = 3.35,$$

$$w(T_{\text{ikK}}) = w_0 \frac{1 + w_1 T_{\text{ikK}}/T_{\text{ckK}}}{1 + w_2 T_{\text{ikK}}/T_{\text{ckK}}},$$

where  $T_{\text{ikK}}$  is ion temperature in kK,  $T_{\text{ckK}} = 7.8$  is critical temperature of gold in kK,  $T_{\text{mkK}} = 1.337$  is melting point,  $w_0 = 0.0043$ ,  $w_1 = 126$ ,  $w_2 = 0.86$ .

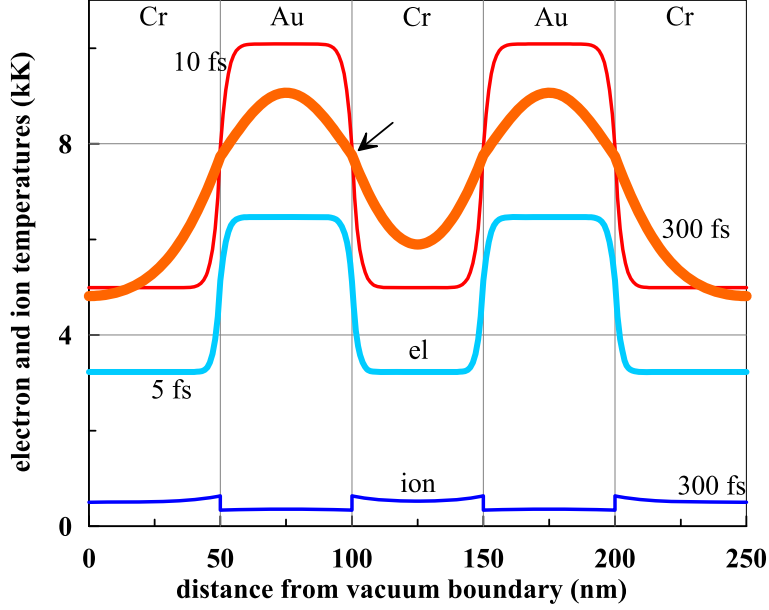


**Figure 8.** The initial part of 2T stage for heating by a “weak” x-ray pulse.

The final expression, which takes into account the scattering of s-electrons on the s- and d-electrons and on ions, is

$$\kappa(T_{\text{ekK}}, T_{\text{ikK}}) = (S_{se} + 1/\kappa_{si}|_{\text{liq}})^{-1}. \quad (5)$$

Here the thermal conductivity coefficient is obtained in units of  $\text{WK}^{-1}\text{m}^{-1}$ . The corresponding plots are shown in figure 6.

We find also the electron coefficient of temperature conductivity as

$$\chi(T_{\text{ekK}}, T_{\text{ikK}}) = \frac{\kappa(T_{\text{ekK}}, T_{\text{ikK}})}{c_e(T_{\text{ekK}})},$$

where  $c_e$  is defined by the expression (3), and the  $\chi$  is in  $\text{m}^2/\text{s}$ , figure 7 where  $\chi$  is given in  $\text{cm}^2/\text{s}$ .

Heat conductivity of chrome  $\kappa_{\text{Cr}}$  is lower than the heat conductivity of gold  $\kappa_{\text{Au}}$  (5). It is assumed that  $\kappa_{\text{Cr}} = 0.6 \kappa_{\text{Au}}$ .

Cooling time of gold layer by thermal conduction is equal  $t \sim d_f^2/\chi \sim 7$  ps at  $\chi = 3.5 \text{ cm}^2/\text{s}$ . The acoustic time scale of expansion of the gold layer, clamped between layers of chrome, is  $d_f/c_s \approx 16$  ps. For chrome the similar time scale is about 11 ps.

The speed of expansion of the system of 5 layers, if we neglect the resistance of silicon with a small acoustic impedance, is of the order of  $u = pt_s/(\rho_{\text{Au}} d_f + \rho_{\text{Cr}} 1.5 d_f) = 800 \text{ m/s}$  for  $p = 40 \text{ GPa}$ ,  $t_s = 30$  ps. To expand matter twice with such speed the time  $2.5 d_f/u \sim 150$  ps is required.

### 3.5. Electron-ion energy exchange coefficient

We represent the coefficient of the electron-ion energy exchange in gold in the form of

$$\alpha_{\text{Au}}(T_e) = 10^{17} \left( 0.2 + \frac{4.3}{K_a} \frac{T_{\text{eV}}^{3.6}}{1 + T_{\text{eV}}^{3.5} + 0.9 T_{\text{eV}}^{4.1}} \right). \quad (6)$$

Here the value of  $\alpha_{\text{Au}}$  is in units of  $\text{WK}^{-1}\text{m}^{-3}$ , and  $T_{\text{eV}}$ —electron temperature in eV. Till now discussions concerning value of  $\alpha_{\text{Au}}$  (6) continue.

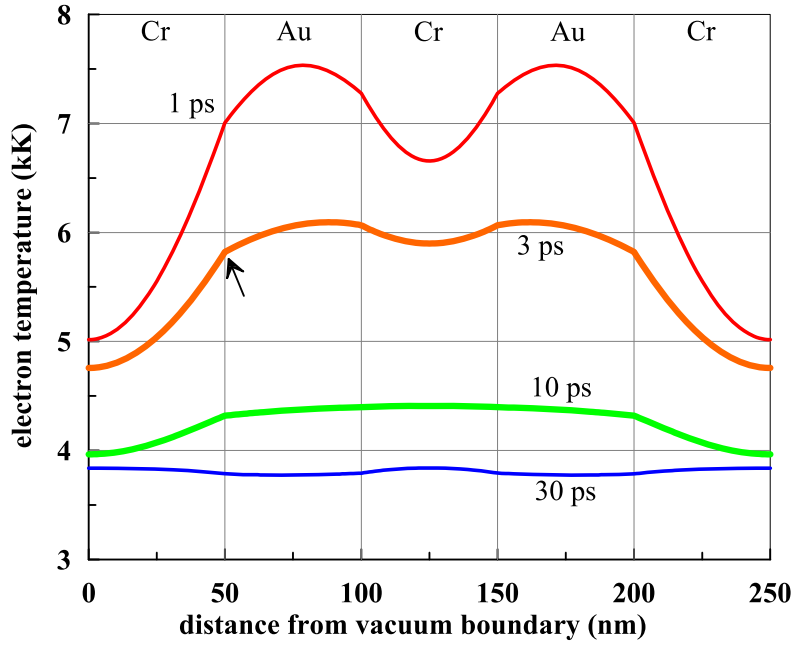


**Figure 9.** The gradual completion of energy transfer stage by the thermal conductivity between Au and Cr layers for the heating by a “weak” pulse. The general decrease in temperature  $T_e$  due to transmission the energy of the electrons to the ions. The arrow notes gradient jump  $\nabla T_e$ .

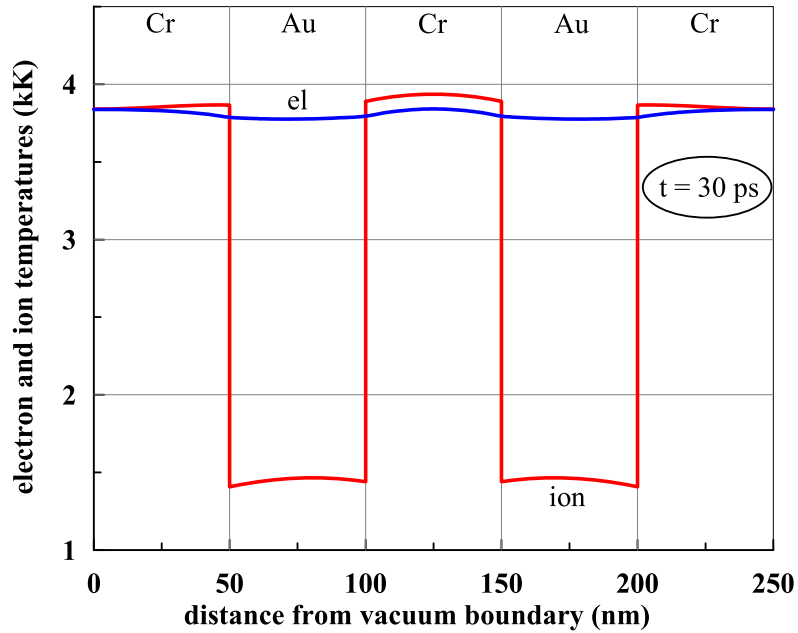


**Figure 10.** The final stage of the thermal relaxation for the heating by a “weak” pulse. Further evolution of heat begins to be distorted due to the hydrodynamic expansion.

The variation of coefficient  $K_a$  within the range 1.15–4 covers uncertainty of  $\alpha_{Au}$ . The value of  $K_a = 1.15$  corresponds to a situation with a large growth of  $\alpha_{Au}$  at heating above  $\approx 5$  kK, and at  $K_a = 4$  growth of  $\alpha_{Au}$  with a temperature  $T_e$  is considerably more moderate.

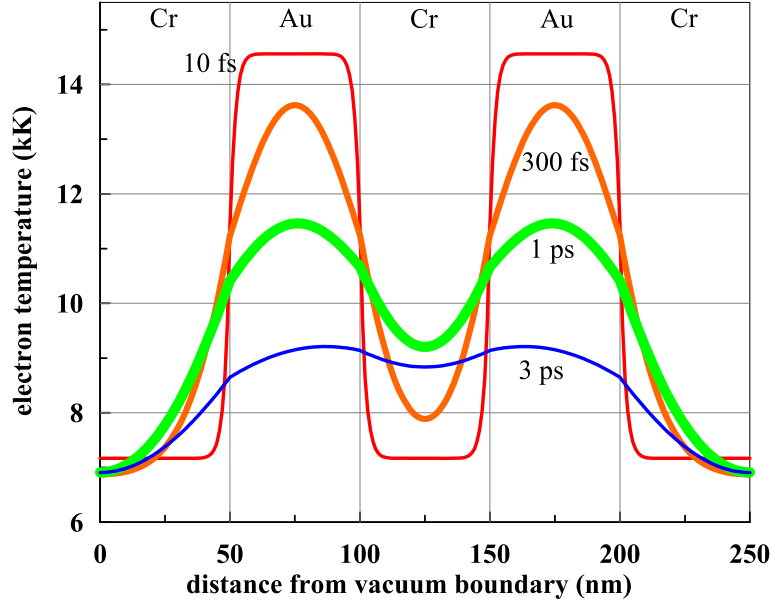


**Figure 11.** “Healing” of two hillocks on  $T_e$  together with decrease  $T_e$  for the heating by a “strong” pulse.

The coefficient  $\alpha_{Cr}$  is great in chrome. We assume that  $\alpha_{Cr} = 3 \times 10^{17} \text{ WK}^{-1} \text{ m}^{-3}$ . Silicon is described by 1T approach in our model.

In particular the difference in coefficients  $\alpha$  between gold and chrome is responsible for a fast relaxation  $T_e \rightarrow T_i$  in chrome and slow one in gold. Due to this at the stage of e-i relaxation the ion temperature of chrome rises faster than the ion temperature of gold. Although immediately after 10 fs of x-ray pulse heating the electron temperature is above in gold.

#### 4. The results for the evolution of the thermal field

The thermal evolution calculations were performed for two heating powers, weak and strong:  $P = 1.37 \times 10^{24}$  and  $2.42 \times 10^{24} \text{ W/m}^3$ . Figure 8 shows the initial stage of the process in a layered target;  $K_a = 4$ . Calculations show that the heat transfer in the silicon substrate is small at our time scale up to  $\sim 100$  ps. The silicon substrate absorbs a little heat and results in a little effect on evolution. If we ignore the small cooling of Au–Cr 5 layer structure due to abutment to the silicon, the temperature field is symmetrical about a median plane passing through the center of the chrome layer in the middle of 5 layers.

Times 5 and 10 fs in figure 8 are attributed to the middle and end of the heating x-ray pulse. Due to the non-linearity of the electron heat capacity (3), the electron temperature grows not proportionally to the absorbed energy to a given time. The arrow in figure 8 marks a kink (gradient jump) of continuous profile of temperature  $T_e$  connected with a difference in coefficients of heat conductivity of gold and chrome, see section 3.4. In the early stages (up to about a picosecond) the gradient of  $T_e$  is great, and time is short, and the the electron heat conduction plays a main role in redistribution of energy. Under the influence of the heat conduction a gap in the temperature  $T_e$  in chrome layers is “healed”, compare the profiles at 10 and 300 fs in figure 8.

On subpicosecond stage the energy transfer from the electron subsystem to the ion subsystem only begins to affect the ion temperature of gold and chrome, see the  $T_i(x, t = 300 \text{ fs})$  profile in figure 8. Paradoxically, although the electron temperature is lower in chrome, the ion temperature is higher in chrome! Alternating ion temperatures in gold and chrome are inverse

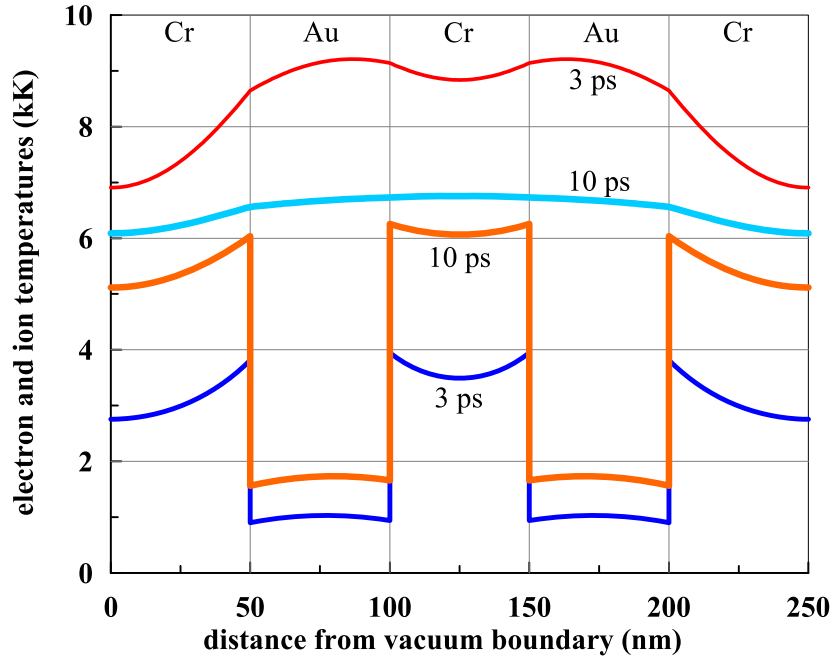


**Figure 12.** The weakening of gradient  $\nabla T_e$  and temperature relaxation for the heating by a “strong” pulse. Two upper curves give  $T_e$ , while the bottom deep blue and orange curves correspond to  $T_i$ .

to the alternating electron temperatures.

The profiles shown in figure 9, through several picoseconds are transformed to profiles in figure 10. The gradient of electron temperature is small, nevertheless the heat conductivity is still acting. Acting, but in the opposite direction. The heat is carried by electron subsystem from gold to chrome after primary heating of electrons of gold by 10 fs pulse, but now the heat flux flowing from chrome to gold. The matter is that the ion temperature of chrome above, see figure 10. The electron temperature  $T_e$  has intermediate values between the ion temperatures  $T_i$  in chrome and in gold. And  $T_e$  is closer to  $T_i$  in chrome, as in chrome the exchange coefficient  $\alpha$  is larger, see subsection 3.5.

At the final stage the electrons take heat from the hotter ion subsystem of chrome, and by conduction, transfer this heat to the cold ion subsystem of gold, see. figure 10. Of course, in a static system, it eventually leads to equalization of ion temperatures of gold and chrome. But the gradient is small, the coefficient  $\kappa$  is also rather small at small  $T_e$  and equalization goes slowly. Therefore in a dynamic situation the equalization process of  $T_i$  between Au and Cr has no time to come to the end. It is caused by the expansion of the layers at times 30–50 ps. In connection with this expansion we call the pattern shown in figure 10 as final one in relation to the thermal evolution.

Let’s consider a situation with the increased input of x-ray energy in 5 layer system: power heating  $P = 2.42 \times 10^{24} \text{ W/m}^3$ , still  $K_a = 4$ , during 10 fs, see subsection 3.5. Initial and average stages of the evolution of electron temperature (from 10 fs to 3 ps) are shown in figure 11. The time 10 fs refers to the end of the heating x-ray pulse, so the temperature  $T_e$  in gold has a maximum. It significantly exceeds the value  $T_e$  at time 10 fs in the case of “weak” pulse, compare figure 8: 14.6 kK against 10.1 kK.

Figure 11 shows how the electron temperature evolves under the effect of heat conduction and energy transfer into the ions. As mentioned above, the thermal conductivity dominates at

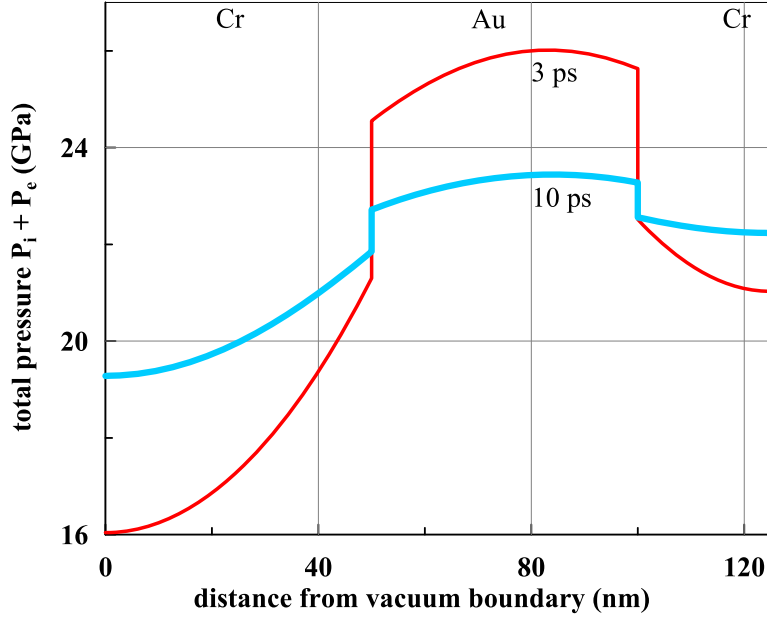


**Figure 13.** Instant pressure distribution on times smaller than acoustic time scale for the heating by a “strong” pulse. The symmetrical half of picture is shown. Pressure in gold is higher, therefore it expands faster and compresses chrome. Furthermore, there is an expansion associated with all layers.

the initial part, and in the final—the heating of ions by the term  $\alpha (T_e - T_i)$  in the system of equations (1) and (2). Heat conductivity mainly smoothes the originally angular profile of  $T_e$ . While the  $\alpha$  term mainly reduces  $T_e$ .

Figure 12 shows the final stage of evolution at which it is still possible to use a static model (1) and (2) without taking into account hydrodynamics. There is a convergence of temperatures  $T_e$  and  $T_i$ . As mentioned above, there are two final stages in the static model. On the end of first stage the gradient  $\nabla T_e$  falls and temperatures  $T_e$  and  $T_i$  in chrome become equal. This is due to the fact that at such values of  $T_e$  the coefficient  $\alpha$  (6) in chrome is several times greater than in gold. On the end of second stage there is an equalization of temperatures of gold and chrome. The first stage end is achieved at times several smaller the acoustic time scale on layer thickness  $d_f = 50$  nm. To wait for a second stage end a time is required, which is significantly higher than the acoustic time.

Note that in the films, where there is no cooling of the surface layer due to heat transfer to the target volume, then the initial temperature  $T_e$  exceeds not strongly the final temperatures. This is due to the fact that at our temperatures  $T_e$  the electron heat capacity and the Dulong–Petit heat capacity  $3 k_B$  are of the same order according to figure 4.

Figure 13 shows the distribution of pressure at the two times. The gold ion and electron pressures are found at temperatures  $T_i$  and  $T_e$  and equations  $p_{\text{liq}|i} = 2.934 T_{\text{kk}|i} + 11.1$  are from the section 3.3 and (4).

In conversion of energy  $\varepsilon_e$  (4) to electron pressure  $p_e$  we put the electron Grüneisen parameter  $\Gamma_e$  equal to one [29]. Pressure in chrome is calculated as follows. First, we determine the energy of the ion subsystem  $\varepsilon_{\text{liq}}(T)|_{\text{Cr}|i} = 1.84 T_{\text{kk}|i} + 3$ , see 3.3. Ion contribution to chrome pressure is calculated by this energy and with the unusually small chrome Grüneisen parameter of  $\Gamma_i = 0.9$ , see [30]. Electron pressure is found from the electron energy in chrome and electron Grüneisen parameter of chrome  $\Gamma_e \approx 1$ . Resulting pressure distributions are shown in figure 13.

## 5. Conclusion

The thermal history of a multi-layered system heated by hard x-ray pulse is studied. We demonstrated that the nontrivial distribution of temperature and pressure in the layers is formed due to the difference in absorption coefficients of the materials of layers and their characteristics at a two-temperature stage. As a result the expansion occurs non-uniformly, where the layer with a high pressure expands stronger squeezing the neighbor layers with less pressure.

## Acknowledgments

We thank K P Migdal for the calculation of the electron spectrum of chrome.

This work was partially supported by the Russian Foundation for Basic Research, project No. 16-08-01181.

## References

- [1] URL <http://xfel.riken.jp>
- [2] URL <http://www.desy.de>
- [3] Inogamov N A *et al* 2011 *Contrib. Plasma Phys.* **51** 367–74
- [4] Petrov Yu V, Inogamov N A and Migdal K P 2013 *JETP Lett.* **97** 20–7
- [5] Migdal K P, Petrov Y V and Inogamov N A 2013 *Proc. SPIE* **9065** 906503
- [6] Petrov Yu V, Migdal K P, Inogamov N A and Anisimov S I 2016 *JETP Lett.* **104** 431–9
- [7] Eidmann K, Meyer-ter-Vehn J, Schlegel T and Hüller S 2000 *Phys. Rev. E* **62** 1202–14
- [8] Inogamov N A, Zhakhovsky V V, Khokhlov V A, Demaske B J, Khishchenko K V and Oleynik I I 2014 *J. Phys.: Conf. Ser.* **500** 192023
- [9] Inogamov N A *et al* 2014 *J. Phys.: Conf. Ser.* **510** 012041
- [10] Thomas D A, Lin Z, Zhigilei L V, Gurevich E L, Kittel S and Hergenroeder R 2009 *Appl. Surf. Sci.* **255** 9605–12
- [11] URL <http://henke.lbl.gov>
- [12] Wagner C and Harned N 2010 *Nat. Photon.* **4** 24–6
- [13] Basko M M, Krivokorytov M S, Vinokhodov A Yu, Sidelnikov Yu V, Krivtsun V M, Medvedev V V, Kim D A, Kompanets V O, Lash A A and Koshelev K N 2017 *Laser Phys. Lett.* **14** 036001
- [14] Inogamov N A, Zhakhovskii V V and Khokhlov V A 2015 *JETP* **120** 15–48
- [15] Wang X W *et al* 2017 *Phys. Rev. Appl.* (arXiv:1703.06758 [cond-mat.mtrl-sci])
- [16] Anisimov S I, Kapeliovich B L and Perel'man T L 1974 *Sov. Phys. JETP* **39** 375–7
- [17] Povarnitsyn M E, Itina T E, Sentis M, Khishchenko K V and Levashov P R 2007 *Phys. Rev. B* **75** 235414
- [18] Povarnitsyn M E and Itina T E 2014 *Appl. Phys. A* **117** 175–8
- [19] Khokhlov V A, Inogamov N A, Zhakhovsky V V, Shepelev V V and Il'nitsky D K 2015 *J. Phys.: Conf. Ser.* **653** 012003
- [20] Khokhlov V A, Inogamov N A, Zhakhovsky V V, Il'nitsky D K, Migdal K P and Shepelev V V 2017 *AIP Conf. Proc.* **1793** 100038
- [21] Lin Z, Zhigilei L V and Celli V 2008 *Phys. Rev. B* **77** 075133
- [22] Petrov Yu V and Inogamov N A 2013 *JETP Lett.* **98** 278–84
- [23] Babar S and Weaver J H 2015 *Appl. Optics* **54** 477–81
- [24] URL <http://www.faculty.virginia.edu/CompMat/>
- [25] Khishchenko K V, Tkachenko S I, Levashov P R, Lomonosov I V and Vorobev V S 2002 *Int. J. Thermophys.* **23** 1359–67
- [26] Levashov P R, Khishchenko K V, Lomonosov I V and Fortov V E 2004 *AIP Conf. Proc.* **706** 87–90
- [27] Khishchenko K V 2008 *J. Phys.: Conf. Ser.* **98** 032023
- [28] Khakshouri S, Alfe D and Duffy D M 2008 *Phys. Rev. B* **78** 224304
- [29] Petrov Yu V, Migdal K P, Inogamov N A and Zhakhovsky V V 2015 *Appl. Phys. B* **119** 401–11
- [30] Girifalco L A 2000 *Statistical Mechanics of Solids (Monographs on the Physics and Chemistry of Materials vol 58)* (Oxford: Univ. Press)